Final Report

Volume 1

Radar Studies of the Moon

31 August 1967

Issued 19 October 1967

Prepared for the U.S. National Aeronautics and Space Administration under Contract NSR 22-009-106 by

Lincoln Laboratory

MASSACHUSETTS INSTITUTE OF TECHNOLOGY

Lexington, Massachusetts

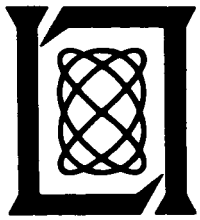

PRECEDING PAGE BLANK NOT FILMED.

FOREWORD

This report has been prepared as part of the final report required under Contract NSR 22-009-106 between the National Aeronautics and Space Administration and M. I. T. Lincoln Laboratory. The measurements and analysis stipulated in the contract separate rather naturally into three parts: (1) the statistical scattering and polarization properties at several wavelengths of the mean lunar surface, (2) the local variations in these properties along the "Apollo belt" associated with different types of lunar surface, and (3) a comparative analysis of the results obtained under the present contract and those to be obtained at longer wavelengths under Grant NGR 33-010-024 between NASA and Cornell University. The latter grant terminates 31 December 1967.

In order to make results obtained under the present contract available as rapidly as possible, it has been decided to serialize the final report in three volumes corresponding to the areas of investigation described above. Thus, the present report constitutes Vol. 1 of the final report and deals with those experiments which have provided information about the average properties of the lunar surface as well as with their interpretation. Volume 2 will present the results of a detailed mapping of the lunar surface radar reflectivity at 3.8-cm wavelength and will be issued as soon as the full results are available. Volume 3, a report to be prepared jointly with Cornell University, will be prepared immediately following the termination of the Cornell grant.

PRECEDING PAGE BLANK NOT FILMED.

CONTENTS

RADAR STUDIES OF THE MOON

I. INTRODUCTION

This report presents and reviews part of the results of a study program to assess the properties of the lunar surface from the earth by radio waves. Only those results which pertain to the mean properties of the lunar surface are considered in this volume. Results which reveal physical differences between local regions on the moon will be the subject of a second volume to be issued in the near future.

The discussion in this report is broken up into three main areas: the total radar cross section of the moon, the distribution of the radar echo power in delay and polarization, and the radiometric observation of the natural lunar thermal emission. In each of these areas observations carried out under the contract are presented in the context of previous work and are examined for their implications as to the structure and properties of the lunar surface.

Although the theoretical derivations and discussions are reasonably complete, they are not exhaustive, nor was it felt desirable to include here a complete bibliography. A good working set of recent references is given by Hagfors (1967), and an even more complete list by Evans (1965). References to QPR (year:number) in the text of this report refer to the Quarterly Progress Reports which have been issued under this contract over the past two years.

II. RADAR CROSS SECTION

A. Observations

As a part of the studies undertaken in this contract, the total cross section of the moon has been measured at 23 cm with high precision. Inaccurate knowledge of the radar system parameters has in the past been the major contributing factor to the uncertainties in the lunar radar cross section. However, use of the Lincoln Calibration Sphere [QPR (1966:2)], an orbiting satellite specifically designed for radar calibration, has greatly reduced these uncertainties. The cross section at 23 cm was found to be (Evans and Hagfors, 1966)

$$\sigma_o = (0.065 \pm 0.008)\, \pi a^2 \qquad (1)$$

where a is the radius of the moon. This value was determined using circularly polarized illumination and by observing the orthogonal (symmetrically reflected) sense of circular polarization on reception. Measurements with comparable accuracy at other wavelengths have not been accomplished primarily because of difficulties with the tracking of the calibration sphere. The most current data on the lunar cross section as a function of wavelength are shown in Fig. 1 expressed as a fraction of the geometrical cross section of the moon. The appropriate references may be found in QPR (1966:1).

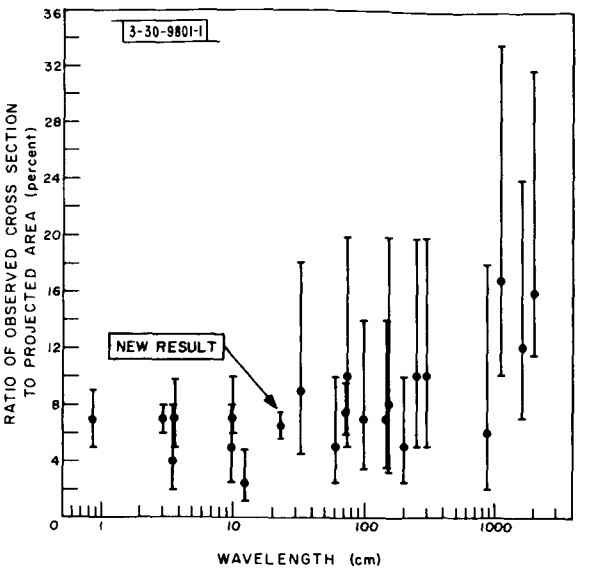

Fig. 1. Cross section of moon vs wavelength with new result at 23 cm added.

B. Interpretation

If the moon were a perfectly smooth sphere, whose surface is composed of a metallic or slightly lossy dielectric, the cross section would be

$$\sigma_o = \rho_o \pi a^2 \tag{2}$$

where ρ_o is the power reflection coefficient at normal incidence to the surface. When the surface is no longer an ideally smooth sphere, but one which deviates from the spherical shape while remaining smooth locally, the cross section is modified to

$$\sigma = \sigma_o(1 + \alpha^2) \tag{3}$$

where α is a measure of the rms slope of the surface undulations. As explained in detail below it has been found that α is small enough so that it can be neglected in comparison with unity.

It has become evident – particularly from extensive polarization measurements – that the return from the moon cannot be completely described as a reflection from a locally smooth, gently undulating surface. It has been found that the reflection must be thought of as originating in two different mechanisms: one which is associated with quasi-specular reflection from the gently undulating surface, and a second which arises as a result of a somewhat more vaguely defined small-scale diffuse scattering mechanism. On the basis of studies of the power returned as a function of the angle of incidence, the amount of diffuse power has been estimated to be approximately as shown in Table I for the various wavelengths examined. It must be pointed out that the estimates given in Table I are crude. Other extrapolation methods may give values considerably less than those quoted. For example, Pettengill and Thompson (1967) have arrived at 12 percent for their 70-cm results.

The presence of a nonspecular backscattering surface component will remove a fraction χ of the surface available for quasi-specular scattering. The total backscattering cross section may therefore be expressed as

$$\sigma = \sigma_o(1 - \chi) + \chi \cdot \sigma_d \tag{4}$$

TABLE I PERCENT OF TOTAL POWER IN DIFFUSE RETURN	
λ (cm)	Percent
68	20
23	25
3.6	35
0.86	85

where σ_d is usually referred to as the cross section of the diffuse component. This cross section may be expressed in terms of a mean spherical albedo $\bar{\rho}$ and a backscattering gain factor G_m:

$$\sigma_d = G_m \cdot \rho \cdot \pi a^2 \quad . \tag{5}$$

Since radar observations so far have been confined to the monostatic case, there is no way of knowing the spherical albedo of the diffuse component nor the backscattering gain factor G_m. Kerr and Shain (1951) deduced a value of G_m of 5.7 at optical wavelengths whereas Grieg, et al. (1948) deduced a gain of 2.7 on the basis of Lambertian scattering from the surface. Assuming, primarily for lack of a better estimate, that mean spherical albedo $\bar{\rho}$ is equal to the specular power reflection coefficient at normal incidence, the fraction χ of the surface responsible for diffuse scattering comes out to be 8.5 percent at 23-cm wavelength. Because of all the assumptions involved this number should only be taken as a very crude estimate.

It has been customary in the past [e.g., Evans and Pettengill (1963)] to assume that the reflection coefficient ρ_o is identical to the Fresnel reflection coefficient at normal incidence. This, of course, assumes that the surface can be represented as a sharp boundary between vacuum and a homogeneous material with certain electrical properties. On this assumption we have

$$\rho_o = \left| \frac{\sqrt{\epsilon} - 1}{\sqrt{\epsilon} + 1} \right|^2 \tag{6}$$

where ϵ is the (complex) relative dielectric constant of the lunar surface material. On these assumptions and also assuming negligible losses, the dielectric constant at 23 cm becomes $\epsilon = 2.64$. The dielectric constants at both 3.8 cm and 70 cm are close to that at 23 cm on the basis of the assumptions just spelled out.

Other evidence may indicate that this type of interface is too simple. The top lunar layers have variously been characterized as dust-layers, as ash-flow deposits or as sandy soil. One may, therefore, have reason to believe that there is a gradual change with depth in the electrical properties of the lunar surface material. This variation may take several different forms, two of which we shall examine in some detail here.

Suppose we have a uniform upper layer with a dielectric constant of ϵ_1, and a depth b, and that this upper layer is supported by a semi-infinite homogeneous medium which has a dielectric constant ϵ_2. The power reflection coefficient can then be determined for the normal incidence case to be

$$\rho_o = \frac{\epsilon_1(\sqrt{\epsilon_2} - 1)^2 - (\epsilon_1 - 1)(\epsilon_2 - \epsilon_1)\sin^2(\sqrt{\epsilon_1}kb)}{\epsilon_1(\sqrt{\epsilon_2} + 1)^2 - (\epsilon_1 - 1)(\epsilon_2 - \epsilon_1)\sin^2(\sqrt{\epsilon_1}kb)} \tag{7}$$

where $k = 2\pi/\lambda$ (λ = wavelength in vacuo).

The quasi-specular return may be regarded as a superposition of "glints" from a large number of area elements which are favorably oriented for reflection. The depth b at the position of these elements may be assumed to be distributed at random in accordance with a probability density p(b). The mean normal reflectivity is found as follows:

$$\langle \rho_o \rangle_{avg} = \int_o^\infty p(b)\, \rho_o(b)\, db \tag{8}$$

with $\rho_o(b)$ given by Eq. (7). The actual mean reflection coefficient will depend strongly on the form of the probability density and on the mean depth (b). When the mean depth is either much smaller than or much greater than $\lambda/4\sqrt{\epsilon_1}$, however, the form of p(b) is no longer important and we obtain in the former case

$$\langle \rho_o \rangle_{avg} = \left| \frac{\sqrt{\epsilon_2} - 1}{\sqrt{\epsilon_2} + 1} \right|^2 \tag{9}$$

and in the latter case

$$\langle \rho_o \rangle_{avg} = 1 - \frac{4\sqrt{\epsilon_1 \epsilon_2}}{(\sqrt{\epsilon_2} + 1)(\sqrt{\epsilon_2} + \sqrt{\epsilon_1})} \quad . \tag{10}$$

Hence a thin layer is invisible and a thick layer serves to reduce the reflection from what it would have been in the absence of a top layer. Minimum reflection for a given ϵ_2 occurs when $\epsilon_1 = \sqrt{\epsilon_2}$. Figure 2 shows graphically the relationship between ϵ_1, ϵ_2 and $\langle \rho_o \rangle_{avg}$. As can be

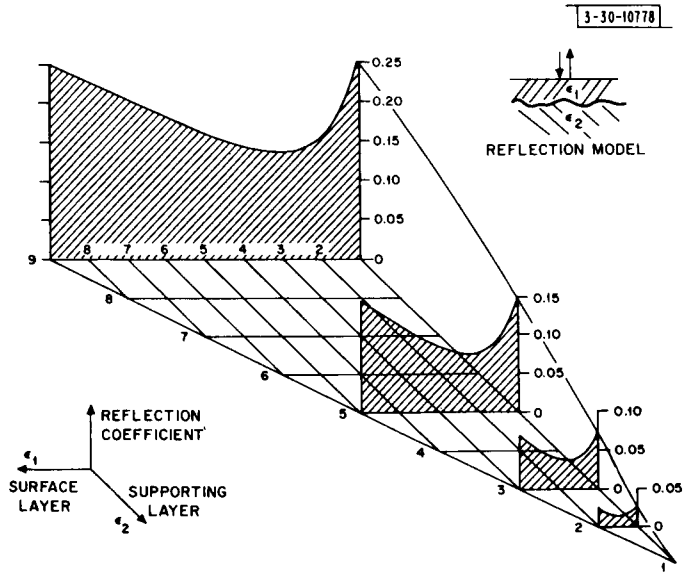

Fig. 2. Power reflection coefficients from dielectric layer of random thickness.

seen, there are many combinations of ϵ_1 and ϵ_2 which can give rise to a required reflection coefficient. On the basis of this model the increase in cross section seen at the longer wavelengths in Fig. 1 may be understood if the depth of the surface layer equals $\lambda/4\sqrt{\epsilon_1}$ for a wavelength between 1 and 10 m. For a crude measure of the depth one may substitute λ = 5 m and $4\sqrt{\epsilon_1}$ = 5 to obtain a depth of one meter.

A model involving a gradual transition in electrical properties through the upper layer may be more realistic. One that can be handled mathematically has a dielectric constant which varies linearly with depth from a value of [redacted] at the top to ϵ_2 at the transition to the underlying layer. The model is shown in Fig. 3. A linear variation in dielectric constant with depth leads to a Stokes differential equation having the two solutions Ai(x) and Bi(x). The reflection coefficient at normal incidence is given by

$$\rho_o = |\mathrm{Det}_-/\mathrm{Det}_+|^2 \tag{11}$$

where

$$\mathrm{Det}_\pm = \left\{\mathrm{Bi}\left(-\frac{\alpha b\epsilon_1}{\Delta\epsilon}\right) \pm \frac{i\alpha}{k}\,\mathrm{Bi}'\left(-\frac{\alpha b\epsilon_1}{\Delta\epsilon}\right)\right\}\left\{\mathrm{Ai}\left(-\frac{\alpha b\epsilon_2}{\Delta\epsilon}\right) - \frac{i\alpha}{k\sqrt{\epsilon_2}}\,\mathrm{Ai}'\left(-\frac{\alpha b\epsilon_1}{\Delta\epsilon}\right)\right\}$$

$$-\left\{\mathrm{Ai}\left(-\frac{\alpha b\epsilon_1}{\Delta\epsilon}\right) \pm \frac{i\alpha}{k}\,\mathrm{Ai}'\left(-\frac{\alpha b\epsilon_1}{\Delta\epsilon}\right)\right\}\left\{\mathrm{Bi}\left(-\frac{\alpha b\epsilon_2}{\Delta\epsilon}\right) - \frac{i\alpha}{k\sqrt{\epsilon_2}}\,\mathrm{Bi}'\left(-\frac{\alpha b\epsilon_1}{\Delta\epsilon}\right)\right\}$$

where

$$\alpha = (k^2\Delta\epsilon/b)^{1/3}$$

$$\Delta\epsilon = \epsilon_2 - \epsilon_1$$

b = depth of layer

$k = 2\pi/\lambda$

λ = wavelength in vacuo .

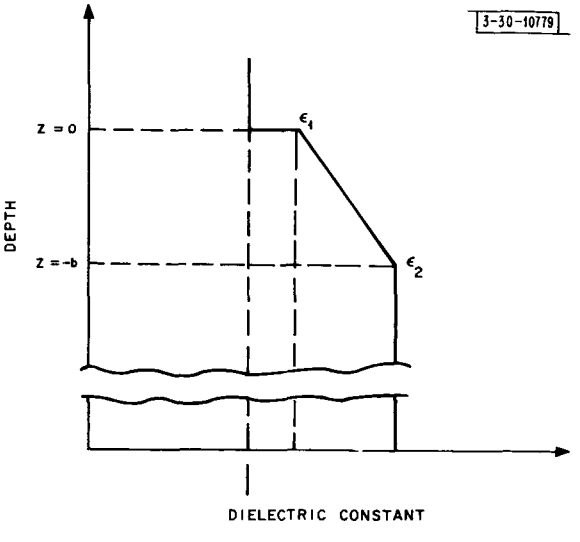

Fig. 3. Model of surface having linear variation of dielectric constant with depth.

TABLE II

RADAR CROSS SECTION PER UNIT SURFACE AREA (db)*

Delay (μsec)	φ (deg)	Wavelength (cm) 3.8	23	68	Delay (μsec)	φ (deg)	Wavelength (cm) 3.8	23	68
10.00	2.38	-0.83	2.77	4.29	2250.00	36.29	-14.18	-16.78	-18.41
20.00	3.37	-1.43	1.92	3.69	2500.00	38.33	-14.58	-17.08	-18.81
30.00	4.12	-1.98	1.37	2.79	2750.00	40.28	-14.88	-17.43	-19.21
40.00	4.76	-2.38	0.87	2.09	3000.00	42.15	-15.23	-17.73	-19.51
50.00	5.32	-2.73	0.42	1.49	3250.00	43.96	-15.53	-18.08	-19.81
60.00	5.83	-3.03	0.02	0.99	3500.00	45.71	-15.83	-18.38	-20.01
70.00	6.30	-3.33	-0.38	0.49	3750.00	47.41	-16.13	-18.63	-20.21
80.00	6.73	-3.58	-0.78	-0.01	4000.00	49.07	-16.38	-18.93	-20.41
90.00	7.14	-3.83	-1.18	-0.51	4250.00	50.68	-16.63	-19.18	-20.61
100.00	7.53	-4.03	-1.53	-0.91	4500.00	52.26	-16.93	-19.58	-20.81
125.00	8.42	-4.58	-2.28	-1.91	4750.00	53.81	-17.13	-19.73	-21.06
150.00	9.22	-5.03	-3.03	-2.71	5000.00	55.32	-17.43	-19.98	-21.31
175.00	9.96	-5.38	-3.68	-3.41	5250.00	56.81	-17.73	-20.28	-21.61
200.00	10.65	-5.73	-4.23	-4.11	5500.00	58.27	-17.98	-20.53	-21.86
225.00	11.30	-6.03	-4.73	-4.71	5750.00	59.71	-18.33	-20.83	-22.16
250.00	11.92	-6.33	-5.23	-5.41	6000.00	61.13	-18.63	-21.08	-22.51
275.00	12.50	-6.68	-5.68	-5.86	6250.00	62.53	-18.93	-21.43	-22.86
300.00	13.06	-6.93	-6.08	-6.41	6500.00	63.92	-19.33	-21.78	-23.21
325.00	13.59	-7.23	-6.43	-6.81	6750.00	65.29	-19.73	-22.18	-23.56
350.00	14.11	-7.48	-6.78	-7.31	7000.00	66.64	-20.13	-22.58	-23.96
375.00	14.61	-7.73	-7.13	-7.61	7250.00	67.98	-20.53	-23.03	-24.36
400.00	15.09	-7.98	-7.43	-8.06	7500.00	69.30	-21.03	-23.43	-24.71
425.00	15.56	-8.23	-7.73	-8.41	7750.00	70.62	-21.43	-23.88	-25.16
450.00	16.01	-8.43	-8.03	-8.71	8000.00	71.92	-21.88	-24.33	-25.66
475.00	16.45	-8.63	-8.43	-9.01	8250.00	73.21	-22.38	-24.83	-26.16
500.00	16.88	-8.78	-8.58	-9.31	8500.00	74.50	-22.88	-25.38	-26.66
600.00	18.51	-9.33	-9.53	-10.31	8750.00	75.78	-23.38	-25.93	-27.21
700.00	20.01	-9.83	-10.43	-11.11	9000.00	77.05	-23.98	-26.53	-27.81
800.00	21.40	-10.23	-11.23	-11.91	9250.00	78.31	-24.53	-27.18	-28.46
900.00	22.72	-10.63	-11.83	-12.61	9500.00	79.57	-25.33	-27.83	-29.06
1000.00	23.97	-10.93	-12.58	-13.31	9750.00	80.82	-26.03	-28.58	-29.76
1100.00	25.15	-11.08	-13.18	-13.96	10000.00	82.07	-26.93	-29.43	-30.61
1200.00	26.29	-11.58	-13.63	-14.61	10250.00	83.32	-27.93	-30.48	-31.61
1300.00	27.39	-11.83	-14.03	-15.21	10500.00	84.56	-29.33	-31.58	-32.61
1400.00	28.44	-12.08	-14.38	-15.71	10750.00	85.80	-30.83	-33.08	-34.06
1500.00	29.46	-12.33	-14.68	-16.11	11000.00	87.04	-32.03	-34.93	-35.81
1750.00	31.88	-13.33	-15.88	-17.51	11250.00	88.27	-32.83	-37.58	-38.41
2000.00	34.15	-13.73	-16.33	-18.01					

* Resolution in delay is approximately 10 μsec.

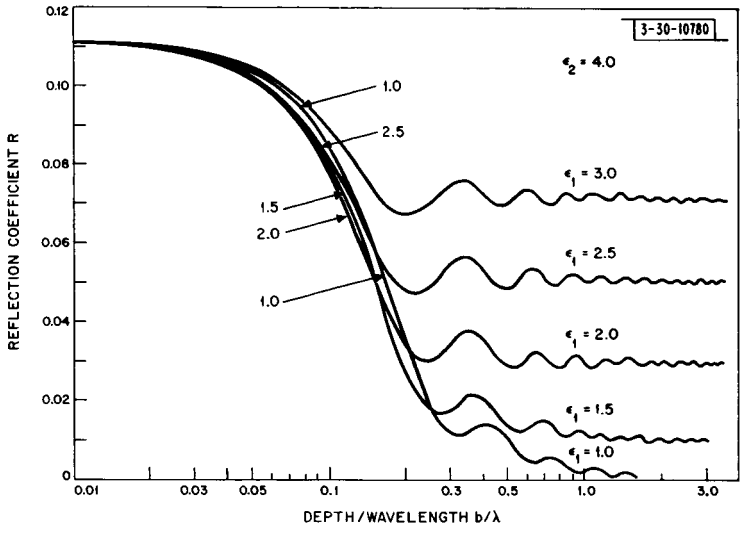

Fig. 4. Reflection coefficient from surface having linear variation of dielectric constant with depth vs layer thickness.

Some computational results for this case are shown in Fig. 4. As can be seen, whenever λ is small compared with the transition region, the reflectivity is determined by the abrupt change in dielectric constant at the top, i.e., by $\epsilon_1 - 1$. We see that the effect of the subsurface will only be observable when $\lambda > 0.26b$.

Other more complicated models can obviously be constructed. One might for instance have an abrupt transition in dielectric constant at z = b (see Fig. 3), and the depth may be random as in the homogeneous double layer model. One may, furthermore, also have to account for possible local variations in the electrical properties of the lunar surface material in computing and interpreting the cross section observations.

The general conclusion which can be reached from this discussion is that the dielectric constant of the upper surface layers is at most 2.64, but that a substantially lower value for these layers would be completely compatible with the cross section data.

III. DELAY DISTRIBUTION OF ECHO POWER

A. Observations

A number of new echo power versus delay measurements have been made at 3.8 cm as well as at 23 cm. At 23 cm these have included observations with circularly polarized and linearly polarized illumination. Observations have been made with both linear and circular polarization on reception. The results of the various experiments are described below with emphasis on wavelength dependence and other clues to the nature of the lunar scattering mechanism.

1. The Polarized Circular Component

Measurements of the power returned as a function of delay have been carried out with good resolution in delay both at 23-cm and at 3.8-cm wavelengths and are given in Table II. The observations have been normalized to a total cross section of 0.065. This is, as explained above, a very accurate value for 23 cm and approximately true at 3.8 cm as well. A value of 0.065 was also chosen for the 68-cm results presented for comparison in Table II, which gives the radar

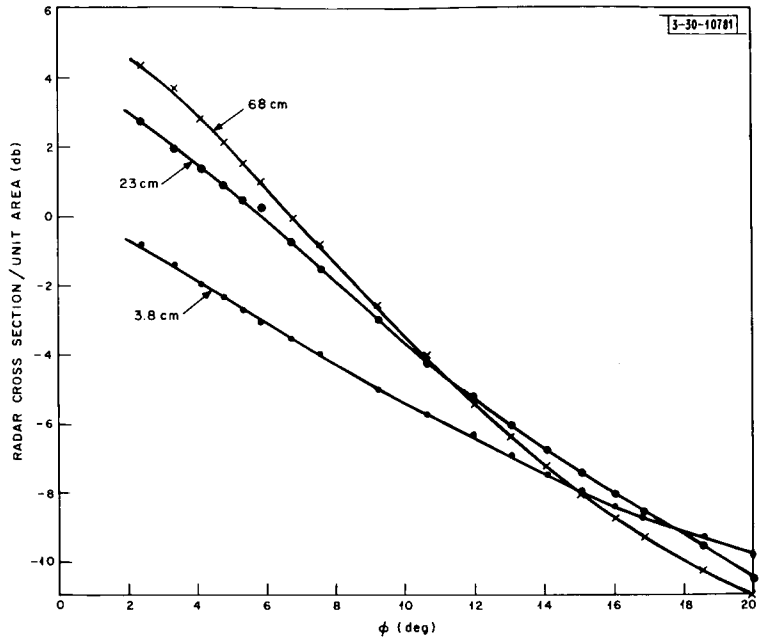

Fig. 5. Cross section per unit surface area vs angle of incidence for small angles; $\lambda = 68$, 23 and 3.8 cm.

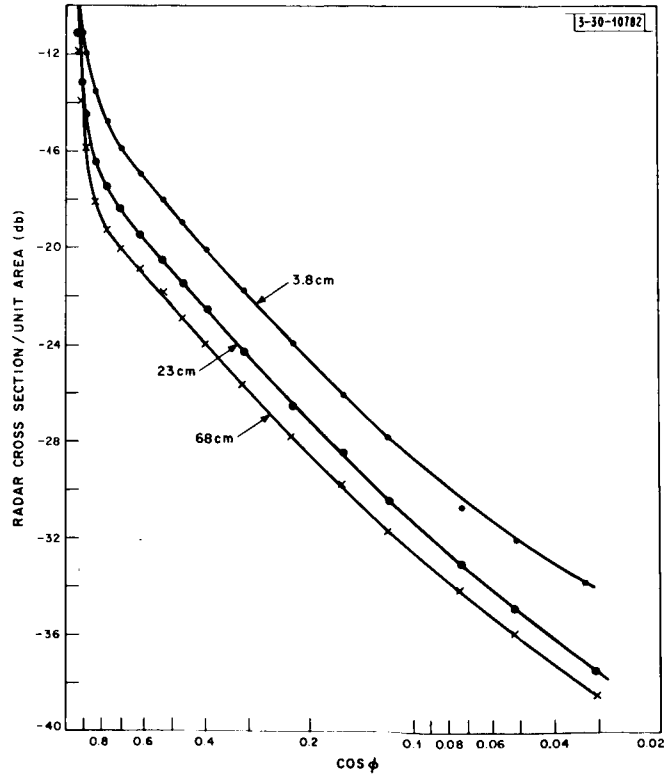

Fig. 6. Cross section per unit surface area vs $\cos\phi$ for large angles; $\lambda = 68$, 23 and 3.8 cm.

cross section per unit area of the surface expressed in db as a function of delay and angle of incidence. In order to show the significance of the data more effectively, the cross sections are plotted as a function of angle of incidence φ for $\varphi < 20°$ in Fig. 5 and for larger φ as a function of $\cos\varphi$ in Fig. 6. It is clearly apparent that there is an appreciable wavelength dependence of the return for small angles of incidence. Near normal incidence the dependence of cross section per unit area on wavelength goes as

$$\left.\begin{aligned} \sigma &\sim \lambda^{0.46} \qquad 3.8\text{ cm} < \lambda < 23\text{ cm} \\ \sigma &\sim \lambda^{0.32} \qquad 23\text{ cm} < \lambda < 68\text{ cm} \end{aligned}\right\} \quad (\varphi \text{ near zero}) \quad .$$

At grazing angles of incidence the wavelength dependence goes in the opposite direction as can be seen from Fig. 6

$$\left.\begin{aligned} \sigma &\sim \lambda^{-0.32} \qquad 3.8\text{ cm} < \lambda < 23\text{ cm} \\ \sigma &\sim \lambda^{-0.26} \qquad 23\text{ cm} < \lambda < 68\text{ cm} \end{aligned}\right\} \quad (\varphi \text{ near normal}) \quad .$$

We also observe that the curves obey a $\cos\varphi^{3/2}$ law for angles φ between 25° and about 80°. For φ larger than 80° a transition to a $\cos\varphi$ dependence appears to take place, at least for the 68- and 23-cm data.

2. The Depolarized Circular Component

Figure 7 shows the expected (polarized) and the depolarized backscattered power at 23 cm plotted as a function of $\cos\varphi$ where φ is the angle of incidence. The relative gain of the two orthogonal channels was checked by means of a linearly polarized target transmitter, as well as by using the radar receivers as radiometers with the moon as a thermal source. The two channels were found to have the same gain to within 10 percent.

The depolarized component decreases more slowly with increasing angle of incidence than does the polarized and may be approximated by a $\cos\varphi$ dependence over a wide range of angles of incidence. The ratio of the two components at 23 cm is shown in Fig. 8 and compared with the corresponding ratio at 68 cm in Fig. 9. No depolarized data are available at a wavelength of 3.8 cm. It appears from Fig. 9 that the depolarization is increasing somewhat with decreasing wavelength.

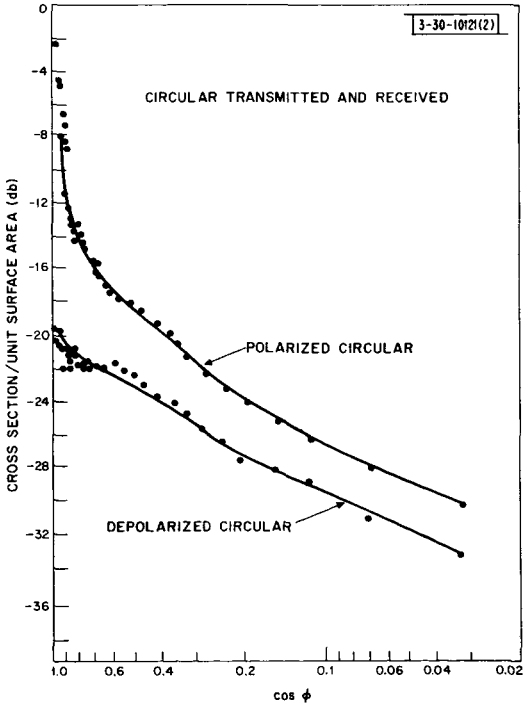

Fig. 7. Cross section per unit surface area at 23 cm for polarized and depolarized circular returns vs $\cos\varphi$.

3. Linearly Polarized Components

The linear depolarization measurements at 23 cm were carried out by transmitting with a fixed, usually vertical polarization. In order to avoid difficulties with Faraday rotation, the linear polarization at the receiver was rotated between

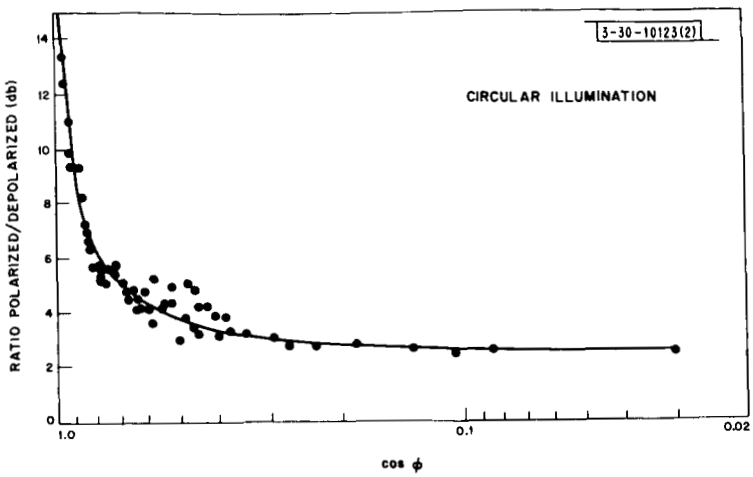

Fig. 8. Ratio of polarized and depolarized returns at 23 cm for circular transmitted polarization vs cosφ.

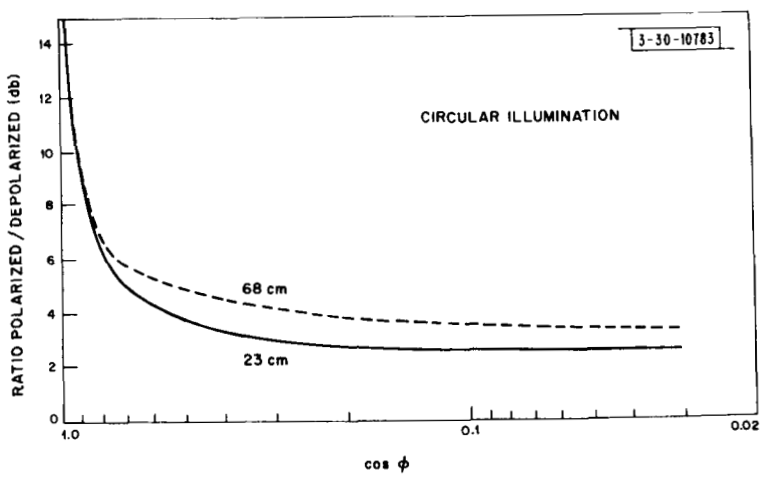

Fig. 9. Comparison of depolarization of circularly polarized returns at 23 and 68 cm vs cosφ.

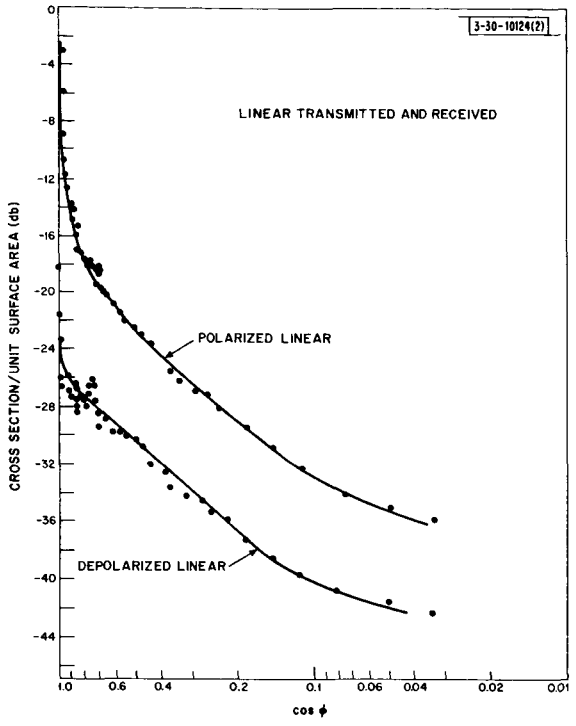

Fig. 10. Cross section per unit surface area at 23 cm for polarized and depolarized linear returns vs cosϕ.

runs. The output power in each polarization would, therefore, vary sinusoidally about a mean level. The least-mean-square sine wave was fitted to the data, and the mean and the depth of modulation were determined to give the total power and the power ratios. Figure 10 shows the polarized and the depolarized linear components again as a function of cos φ. Their ratio is shown in Fig. 11. A comparison of these results with those obtained with circularly polarized waves is made below with the discussion of the data. Comparable results at other wavelengths are not available.

The total power, i.e., the sum of the power in the polarized and depolarized components should be identical functions of the angle of incidence. As a check, the 23-cm total power for the

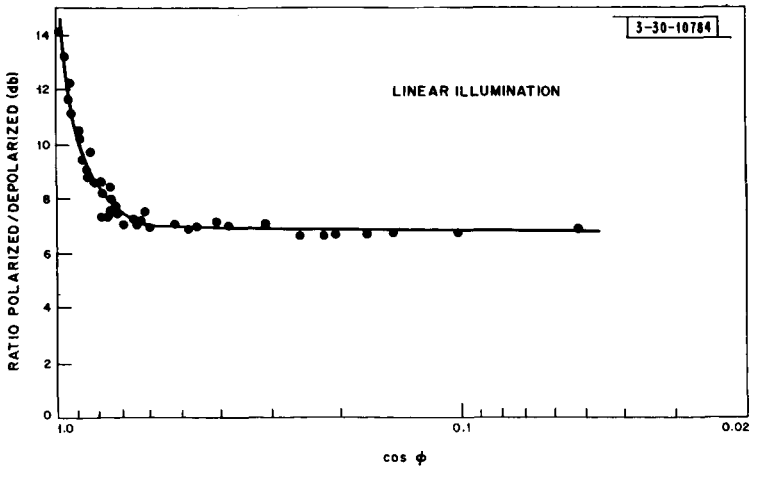

Fig. 11. Ratio of polarized and depolarized returns at 23 cm for linear polarization vs cosϕ.

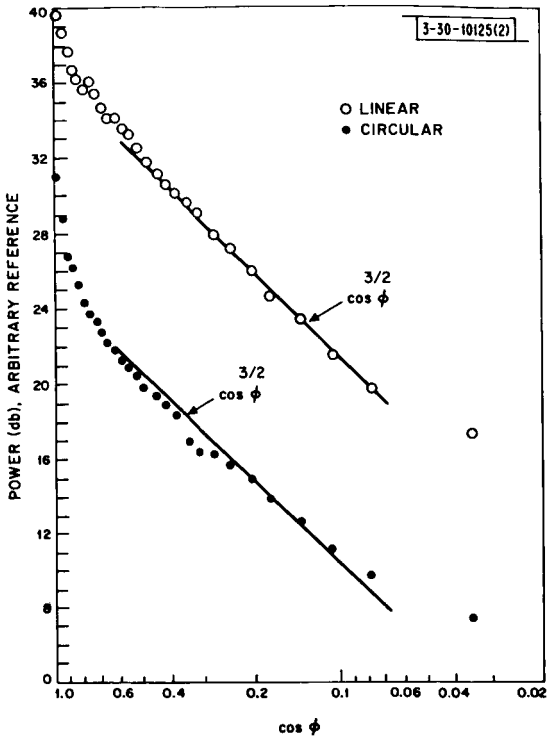

Fig. 12. Comparison of the angular variation of total backscattered power at 23 cm when illumination is circularly and linearly polarized.

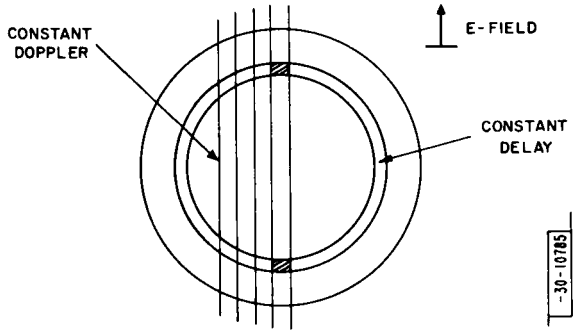

Fig. 13. Method of selecting areas using delay-Doppler resolution where the E-field is aligned with the plane of incidence.

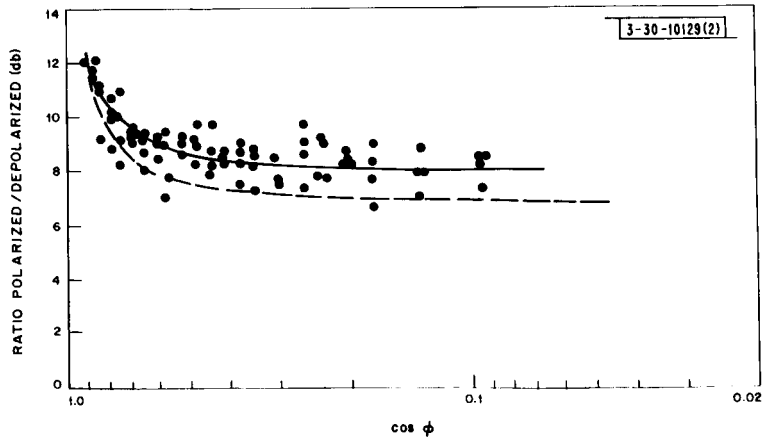

Fig. 14. Ratio of backscattered power at 23 cm in two orthogonal linearly polarized components for linearly polarized illumination with polarization parallel to plane of incidence. Dashed curve shows depolarization when polarization of illumination is averaged over all angles for the same data.

two cases is plotted against $\cos\varphi$ in Fig. 12 and as may be seen, the agreement is reasonable. The total power varies as $\cos\varphi^{3/2}$ to a very good approximation in either case, except near grazing incidence where the angular dependence tends toward $\cos\varphi$.

Since the linear depolarization measurements described so far combine the return from a complete ring of constant delay and hence include all possible directions of the local plane of incidence, the depolarization could possibly arise as a result of different backscattering coefficients for the two principal polarizations. In this case there should be little or no depolarization of a linearly polarized wave with electric field either in or perpendicular to the local plane of incidence. To test this hypothesis the E-field was aligned with the libration axis of the moon as shown in Fig. 13. By Fourier analyzing the data for the Doppler frequency component corresponding to the center of the lunar disk, areas such as the ones shown shaded in Fig. 13 may be selected by delay-gating. In these areas the E-field lies in the local plane of incidence. The polarized/depolarized power ratio observed under these circumstances is shown as a function of $\cos\varphi$ in Fig. 14 for some 23-cm observations. As can be seen there is little difference between these results and the ones obtained as an average over the complete range ring. It is therefore concluded that the depolarization of linearly polarized waves cannot be explained by invoking a difference in the two principal backscattering coefficients. Unfortunately, no similar measurements appear to be available at wavelengths other than 23 cm for comparison.

4. Principal Backscattering Coefficients for Linear Polarization

The ratio of the two principal backscattering coefficients for linearly polarized waves has been measured at both 23 and 3.8 cm. In both sets of observations the transmitted wave was circularly polarized and two orthogonal linearly polarized components of the echo were studied separately. At 23 cm the necessary resolution on the moon was achieved by an application of the delay-Doppler technique as described above [see Hagfors, et al. (1965) for more details]. At 3.8 cm sufficient beam resolution was available to provide the necessary discrimination between different areas. The results of the measurements are shown in Figs. 15 and 16. It can be seen that the ratio of power in the component polarized normal to the plane of incidence to that polarized IN the plane of incidence approaches 0.5 for the 23-cm data and 0.75 for the 3.8-cm data near grazing angles of incidence.

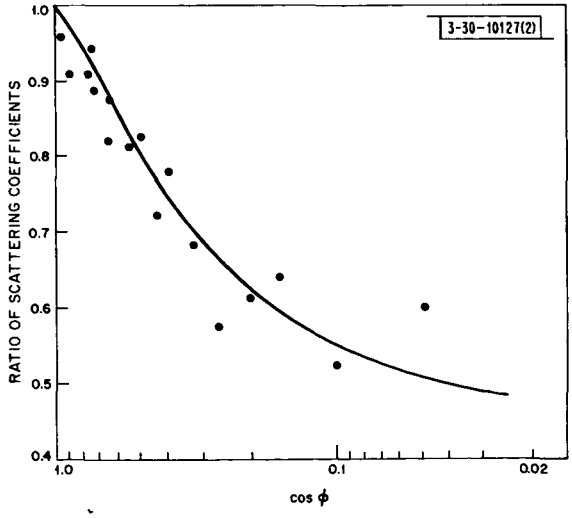

Fig. 15. Ratio of backscattered power at 23 cm in two orthogonal linearly polarized components from a small region of the lunar surface for circularly polarized illumination.

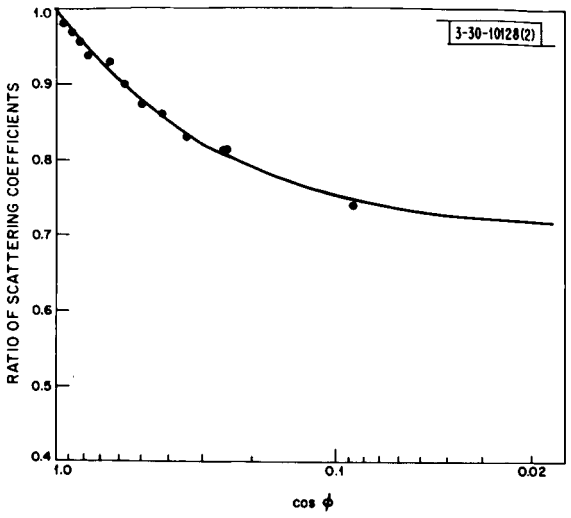

Fig. 16. Ratio of backscattered power at 3.8 cm in two orthogonal linearly polarized components from a small region of the lunar surface for circularly polarized illumination.

B. Interpretation

A uniform brightness over the disk of the moon would give rise to a $\cos\varphi$ variation in the backscattering cross section. Hence only the depolarized returns approximate what one would expect on the basis of a uniformly bright disk. The polarized return at all radio wavelengths exhibits strong aspect sensitivity so that most of the returned power will arise in a region which is near normal to the direction of the radar.

A reasonably good understanding of the angular dependence of the scattering can be obtained by assuming that the boundary condition on the reflecting surface is well approximated by the tangential plane assumption. This assumption involves replacing the surface at any point with a tangential plane and assigning to that point the boundary field which would exist on that tangential plane. The approximation is thought to be a reasonable one for the quasi-specular return, but may not be adequate for the diffuse return nor for the depolarized return. Our view on this, however, is contested by Beckmann (1967).

When the surface is described as quasi-smooth with a reflectivity at normal incidence of ρ_o, and when the surface is assumed to deviate from its mean shape at a point $\vec{r}$ by an amount $h(\vec{r})$ which is a stochastic function of $\vec{r}$, we obtain

$$P_r = P_T \frac{G_R G_T}{8\pi R^4 \cos^2\varphi} \rho_o \cdot \int_o^\infty d(\Delta r)\, \Delta r\, J_o(2k\Delta r \sin\varphi) \cdot \exp\{-4k^2 h_o^2 \cos^2\varphi\, [1-\rho(\Delta r)]\} \qquad (12)$$

where

P_r = received power

P_T = transmitter power

$G_R G_T$ = product of receiver and transmitter gains

R = distance to the moon

$J_o(\,)$ = the zero-order Bessel function

$$k = 2\pi/\lambda$$

$$\rho(\Delta r) = \frac{1}{h_o^2} \langle h(r)\, h(r + \Delta r) \rangle_{avg.}$$

$$h_o^2 = \langle h(r)^2 \rangle_{avg} \quad .$$

For the moon it appears to be safe, based on optical observations of the moon, to assume that

$$2kh_o \cos\varphi >> 1 \tag{13}$$

for all angles and wavelengths of practical interest. As long as $\rho(\Delta r)$ can be expanded about $\Delta r = 0$ in a power series

$$\rho(\Delta r) = 1 - \frac{\Delta r^2}{2} [-\rho''(0)] + \ldots \tag{14}$$

where

$$\rho''(0) = \frac{\partial^2 \rho}{\partial \Delta r^2} \quad , \quad \Delta r = 0$$

and as long as this is a good approximation to the correlation function within the range over which the exponential term is appreciably different from zero, we obtain for the power scattered per unit area at an angle φ

$$P_r = \frac{1}{2\cos^4\varphi\, h_o^2(-\rho'')} \cdot \exp[-\tan^2\varphi/2h_o^2(-\rho'')] \frac{P_T G_T G_R \lambda^2}{64\pi^3 R^4} \quad . \tag{15}$$

This can be shown to be equivalent to the following expression.

$$P_r = \frac{1}{2\cos\varphi}\, p(\varphi)\, \frac{P_T G_T G_R \lambda^2}{64\pi^3 R^4} \tag{16}$$

where $p(\psi)$ is the probability density for the angle ψ between the normal to a surface element and the mean normal to the surface. Under these conditions, which are equivalent to those of geometrical optics, it is a relatively straightforward affair to identify mean slope and rms slope of the lunar surface from the power/delay data. Assume for example that

$$\rho(\Delta r) = \exp(-\Delta r^2/2d_o^2) \tag{17}$$

and hence that

$$-\rho'' = 1/d_o^2 \quad .$$

The rms slope along any direction on the surface is

$$(t_x)_{rms} = (t_y)_{rms} = h_o/d_o \tag{18}$$

The "mean slope" or the mean value of the tangent to the angle between the normal to an arbitrary surface element and the normal to the mean surface becomes

$$\langle \tan\varphi \rangle_{avg} = \left(\frac{\pi}{2}\right)^{1/2} \frac{h_o}{d_o} = 1.25 \frac{h_o}{d_o} \quad . \tag{19}$$

The rms of the tangent to this angle becomes

$$\{\langle \tan^2\varphi \rangle_{avg}\}^{1/2} = \sqrt{2}\,\frac{h_o}{d_o} = 1.41 \frac{h_o}{d_o} \quad . \tag{20}$$

Let us next turn to cases where there is no such simple relationship between true and apparent surface slopes. This occurs whenever the conditions spelled out above are not met. Physically, the breakdown of the conditions means that the surface has a considerable amount of fine structure of a lateral scale not necessarily as small as the wavelength but of a vertical scale smaller than the wavelength of the exploring wave. This will bring about structural detail in the correlation function near the origin which will not appreciably influence the value of the integral [Eq. (12)] determining the backscattered power. This fine structure could, on the other hand, well be completely dominant in determining the true rms slope of the surface. In this situation the slope distribution derived from direct geometric optic analysis can only apply to apparent slopes resulting from the smoothing effect imposed by the scale of the wavelength of the scattered radiation. This smoothing scale, unfortunately, is a function of the angle of incidence of the waves on the surface. To see this it is only necessary to refer again to the integral [Eq. (12)] giving the backscattered power per unit area as a function of angle of incidence φ. When φ is close to zero, the integral is determined primarily by a range of Δr extending from 0 to Δr_e, where Δr_e is the solution of the equation

$$4k^2 h_o^2 \cos^2\varphi\, [1 - \rho(\Delta r_e)] \approx 1 \quad . \tag{21}$$

For somewhat larger angles of incidence φ it will be the Bessel function that limits the range of Δr over which significant contributions to the integral are obtained. The range of Δr as determined by the "width" of the Bessel function extends from 0 to Δr_B, and it is given, at least in order of magnitude, by

$$\Delta r_B \approx \frac{1}{k \sin\varphi} \quad . \tag{22}$$

To relate the range of scales on the surface to the range of separations Δr we can expand $\rho(\Delta r)$ into a power spectrum

$$\rho(\Delta r) = \frac{1}{2\pi} \int_0^\infty \kappa d\kappa F(\kappa)\, J_o(\Delta r, \kappa) \quad . \tag{23}$$

The spectrum of random rough surfaces usually decreases monotonically. As examples, consider the Gaussian autocorrelation function (17) for which we obtain

$$F(\kappa) = 2\pi d_o^2 \exp(-\kappa^2 d_o^2/2) \tag{24}$$

whereas for the exponential autocorrelation function often used [Hughes (1962)], i.e., $\exp(-\Delta r/d_1)$, we obtain

$$F(\kappa) = 2\pi d_1^{-1}(d_1^{-2} + \kappa^2)^{-3/2} \tag{25}$$

Since the fine structure in the correlation function in the range of Δr either from 0 to Δr_e or from 0 to Δr_B cannot appreciably affect the integral in Eq. (12), we conclude that an approximation to the received power is obtained by "filtering" out the high frequency components in Eq. (23) by writing

$$\rho_e(\Delta r) = \frac{1}{2\pi} B \int_0^{\kappa_M} \kappa d\kappa F(\kappa)\, J_0(\Delta r, \kappa) \tag{26}$$

where B is a normalizing constant and

$$\kappa_M = \begin{cases} 1/\Delta r_e & \Delta r_B > \Delta r_e \\ 1/\Delta r_B & \Delta r_B < \Delta r_e \end{cases} \tag{27}$$

This approximation can only be regarded as somewhat crude. A filtering function should have been applied to Eq. (23), and this filtering function would not necessarily have the rectangular shape implied by Eq. (26). For this reason the procedure discussed serves only to illustrate the gradual decrease in the scale of the effective irregularities with increasing angle of incidence. Also, because of the truncation, h_o^2 must be adjusted somewhat to an effective h_e^2 through

$$h_e^2 = h_o^2 \int_0^{\kappa_M} \kappa d\kappa F(\kappa) \Big/ \int_0^{\infty} \kappa d\kappa F(\kappa) = \frac{h_o^2}{B} \quad . \tag{28}$$

For a Gaussian autocorrelation function,

$$\kappa_M = \begin{cases} \dfrac{\sqrt{2} k h_o \cos\varphi}{d_o} & \text{when } \tan\varphi < \sqrt{2}\,\dfrac{h_o}{d_o} \\ k \sin\varphi & \text{when } \tan\varphi > \sqrt{2}\,\dfrac{h_o}{d_o} \end{cases} \quad . \tag{29}$$

As long as κ_M is large in comparison with $1/d_o$ there will be little effect of the truncation, since it makes little difference whether the integration in Eq. (26) is carried to infinity or to κ_M under these circumstances. This condition on κ_M is closely related to the assumption of a deep and gently undulating phase screen, i.e., to $kh_o > 1$ and $h_o/d_o < 1$. For the Gaussian autocorrelation function it is therefore seen that the same range of scales will contribute to the scattered power at all angles of incidence.

In certain situations, however, the power spectrum $F(\kappa)$ decays sufficiently slowly with κ so that the effective autocorrelation function $\rho_e(\Delta r)$ appreciably changes form with κ_M. Since κ_M is increasing with the angle of incidence, the smallest scale of those responsible for backscattering is decreasing with increasing angles of incidence. This in turn brings about an increase in the effective slope with increasing angles of incidence. When this effect is appreciable, the interpretation of the backscattered power as a function of angle of incidence in terms of a geometric optics model [Rea, et al. (1964)] is of doubtful value.

The effective slope of the filtered version of the surface may be defined in analogy with the Gaussian autocorrelation case as follows

$$\frac{h_e^2}{d_{e0}^2} = -h_e^2 \rho_e''(0) = \frac{h_o^2}{4\pi} \int_0^{\kappa_M} \kappa^3 F(\kappa)\, d\kappa \quad . \tag{30}$$

Let us finally outline briefly a procedure which, if realizable, would lead to a somewhat more meaningful estimate of the characteristics of a rough surface. First, we observe that for very small angles φ the scales involved do not change appreciably with φ [see Eq. (24)]. In the region of small φ a reasonably well defined apparent slope on the scale of $2\pi\kappa_M^{-1}$ may therefore be defined by comparison with the Gaussian autocorrelation case. If the observation is repeated at a number of wavelengths in the small φ region, we will be able to define a slope function

$$f(\kappa_M) = \frac{h_e^2}{d_{e0}^2} = \frac{h_o^2}{4\pi} \int_o^{\kappa_M} \kappa^3 F(\kappa)\, d\kappa \quad . \tag{31}$$

The spectrum $F(\kappa)$ can then be determined from

$$F(\kappa) = \text{const}\, \kappa^{-3}\, df/d\kappa \quad . \tag{32}$$

The lunar data, unfortunately, are such that they will not fit a simple model of the geometrical optics type. A reasonably good fit is obtained by using the correlation function of Eq. (25). In this case one obtains for the backscattering cross section per unit surface area

$$\sigma = \frac{C \cdot \rho_o}{2 \cos^6 \varphi} \left(1 + C \frac{\tan^2 \varphi}{\cos^2 \varphi}\right)^{-3/2} \tag{33}$$

where $C = (d_1 \lambda / 4\pi h_o^2)^2$.

Figure 17 represents an attempt to fit the shape of the curves of expression (33) to the data of Table II by adjusting the reflection coefficient ρ_o and the constant C for a best fit.

The data fit expression (33) quite well over a certain range of angles near normal incidence. Best fit is obtained with the parameters shown in Table III.

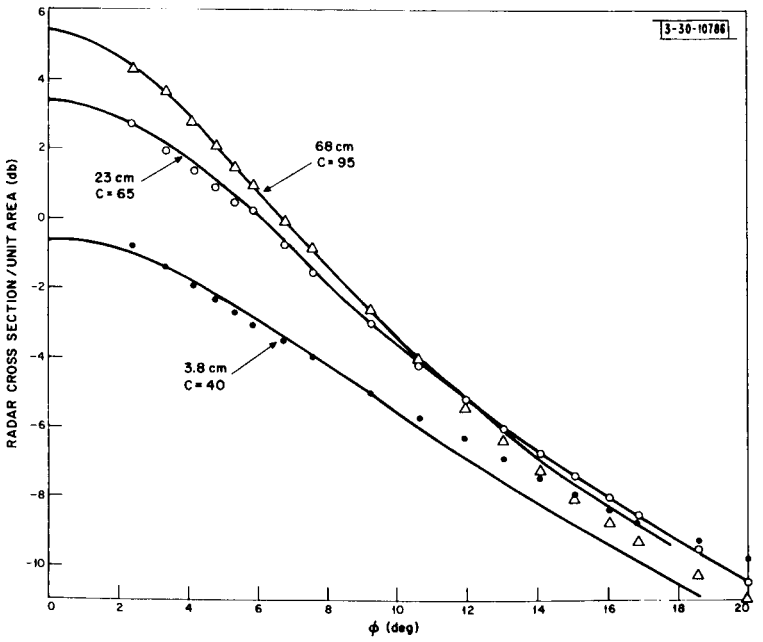

Fig. 17. Fit of data to exponential correlation law at 3.8-, 23- and 68-cm wavelength.

TABLE III

PARAMETERS FOR BEST FIT OF DATA TO THEORY

Wavelength (cm)	C	ρ_o
68	95	0.0697
23	65	0.0648
3.8	40	0.0500

Whereas the fit at 68 and 23 cm is excellent, the fit at 3.8 cm is rather poor and the parameters quoted may therefore be somewhat in error. At 3.8 cm it appears that the simple exponential correlation function is not a very good description of the surface scattering. Obviously, a better fit could be obtained by using a "composite" correlation function of the form [Beckman (1964)]

$$\rho(\Delta r) = \sum_{i=1}^{N} \alpha_i \, e^{-|\Delta r|/d_i} \tag{34}$$

as long as a sufficient number of parameters α_i and d_i are allowed.

We also note that the normal incidence reflection coefficients appearing in the third column of Table III for 68- and 23-cm data are in very good agreement with those derived from total cross section considerations (see Sec. III.A.2).

Since the correlation function which appears to fit the data best for the two longer wavelengths is such that a rms slope cannot easily be assigned to the surface, $\rho''(0)$ being infinite, we apply the theory just outlined to derive a measure of slopes and a spectral resolution for the surface undulations.

For the 68 and 23 cm data where the exponential correlation function appears to provide an accurate description, the solution to Eq. (21) – assuming deep phase modulation – is

$$\frac{1}{\Delta r_e} = \frac{4k^2 h_o^2 \cos^2\varphi}{d_1} = \frac{2k\cos^2\varphi}{\sqrt{C}} = \frac{4\pi\cos^2\varphi}{\lambda\sqrt{C}} \quad . \tag{35}$$

Hence, even for normal incidence, the scales of importance extend down to the size of the wavelength of the scattered wave. The slope function defined in Eq. (31) now becomes

$$f(\kappa_M) = \frac{h_o^2 \cdot \kappa_M}{2d_1} \left[\sqrt{1} + (d_1\kappa_M)^{-2} - (d_1\kappa_M)^{-1}\right]^2 \quad . \tag{36}$$

When $d_1\kappa_M$ is large, as appears to be the case here, we obtain approximately

$$f(\kappa_M) = \frac{h_e^2}{d_{eo}^2} \approx \frac{\cos^2\varphi}{2C(\kappa_M)} \quad . \tag{37}$$

This appears to imply that the angles corresponding to the rms slopes at the scale of 68 and 23 cm, respectively, are 6° and 7°. These values are noticeably lower than the 10° to 12° one would tend

to derive on the basis of geometrical optics. The discrepancy only reflects the difficulty of assigning a slope parameter to the lunar surface structure.

Next we proceed to fit a power law to the spectral function $F(\kappa)$. This can be done with somewhat greater confidence than the assignment of a slope to the surface since the limit of integration κ_M enters in a less critical manner. The fitting procedure results in a law of the form

$$F(\kappa) = \text{const}\,\kappa^{-3.7} \tag{38}$$

for the spectral resolution of the surface undulations in the lateral size region 20 to 70 cm. We are, unfortunately, not aware of any data with which this spectral resolution can be compared.

Let us next turn our attention to data pertaining to oblique angles of incidence, i.e., angles in excess of some 30°. For these angles it does not appear that the smooth undulating surface model is a good one to describe the scattering mechanism. In particular, the polarization data are difficult to explain without invoking the scattering from discrete, individual, wavelength-sized objects strewn over the surface.

The depolarization of circularly polarized scattered waves for circularly polarized illumination may be thought of as arising in at least one of two different ways. There may be a systematic difference in the backscattering coefficients for waves polarized in or perpendicular to the local plane of incidence (the two principal linear polarizations). There may be a depolarization of the two principal linearly polarized waves in the sense that illumination in one principal linear polarization gives rise to scattered power in the orthogonal linear polarization also. The results given in Sec. III.A.3 show that the former of the two possibilities does occur. On the other hand, the results in Sec. III.A.4 show that the latter type of mechanism is also present. In order to evaluate the relative importance of these mechanisms in causing depolarization of circularly polarized waves, we may argue as follows.

Let the backscattering matrix of a surface element be

$$S = \begin{Vmatrix} r_{11} & r_{12} \\ r_{21} & r_{22} \end{Vmatrix} \tag{39}$$

so that the linearly polarized fields in and across the local plane of incidence, E_1 and E_2, respectively, are related to the incident fields E_1' and E_2' through

$$\begin{Vmatrix} E_1 \\ E_2 \end{Vmatrix} = \begin{Vmatrix} r_{11} & r_{12} \\ r_{21} & r_{22} \end{Vmatrix} \begin{Vmatrix} E_1' \\ E_2' \end{Vmatrix} \tag{40}$$

The corresponding connection between circularly polarized waves is

$$\begin{Vmatrix} E_r \\ E_l \end{Vmatrix} = \frac{1}{2} \begin{Vmatrix} r_{11} + r_{22} - i(r_{12} - r_{21}) & , & r_{11} - r_{22} - i(r_{12} + r_{21}) \\ r_{11} - r_{22} + i(r_{12} - r_{21}) & , & r_{11} + r_{22} + i(r_{12} - r_{21}) \end{Vmatrix} \begin{Vmatrix} E_r' \\ E_l' \end{Vmatrix} .$$

The ratio of depolarized to polarized received circular components when the illumination is circular hence becomes

$$\frac{\text{Depol}}{\text{Pol}} = \frac{\langle |r_{11} - r_{22} - i(r_{12} + r_{21})|^2}{\langle |r_{11} + r_{22} + i(r_{12} - r_{21})|^2 \rangle} \quad . \tag{41}$$

In the particular case when $r_{12} = r_{21} = 0$, we obtain

$$\frac{\text{Depol}}{\text{Pol}} = \frac{\langle |r_{11} - r_{22}|^2 \rangle}{\langle |r_{11} + r_{22}|^2 \rangle} \quad . \tag{42}$$

If the phases of the two reflection coefficients are the same, the circular depolarized-to-polarized power ratio may be expressed directly in terms of the ratio of the two principal linear power backscattering coefficients $\rho_{||}$ and $\rho_{\perp}$ as follows

$$\frac{\text{Depol}}{\text{Pol}} = \left(\frac{\sqrt{\rho_{||}} - \sqrt{\rho_{\perp}}}{\sqrt{\rho_{||}} + \sqrt{\rho_{\perp}}} \right)^2 \quad . \tag{43}$$

Figure 18 shows a plot of the expected ratio of depolarized and polarized power for circular polarization as a function of the ratio $\rho_{||}/\rho_{\perp}$. Note that in this case there would be no depolarization of the two principal linearly polarized components. We also note that a systematic phase difference of the two reflection coefficients $\rho_{||}$ and $\rho_{\perp}$ would lead to a preferential circular polarization of the scattered wave for linearly polarized illumination. This possibility was excluded at the outset of our discussion as being physically implausible.

Figure 18 shows that the difference in the reflection coefficients $\rho_{||}$ and $\rho_{\perp}$ actually observed (see Figs. 15 and 16) is inadequate to account for the depolarization of circularly polarized waves. It is, therefore, concluded that the fact that r_{12} and r_{21} are nonzero, as indicated by the observational results shown in Fig. 14, must also be an important factor in producing depolarization.

In order to continue the discussion it is convenient at this point to introduce a specific model which may be adjusted to reproduce the observed data. Imagine that the backscattering arises in part from specular reflectors which do not depolarize at all. This type of mechanism clearly is dominant near the subradar point, as indicated previously. With increasing angles of incidence we postulate that the scattering occurs increasingly from a discrete structure which acts as single scatterers. These discrete scatterers may, as a

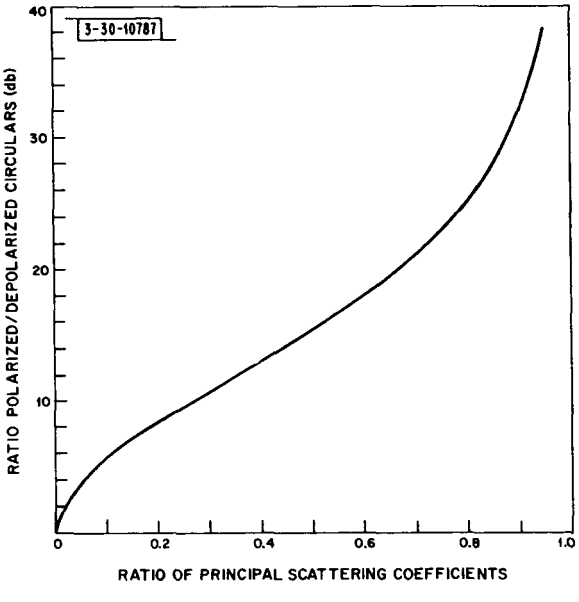

Fig. 18. Plot of ratio of polarized and depolarized power for circularly polarized illumination as a function of the ratio of the backscattering coefficients of the two principal linear polarizations.

first approximation, be thought of as linear dipoles of more or less random orientation. The assumption of single scattering rather than multiple scattering to account for the polarization effects is well justified by the very low reflectivity of the lunar surface material.

A linear dipole will depolarize a circularly polarized wave completely, i.e., the energy scattered in right and left polarizations will be of equal strength. By observing the ratio of polarized to depolarized power as above, it is, therefore, possible to estimate the relative amount of power P_r scattered by the reflection mechanism, and the power P_S by the dipole scatter mechanism. The ratio of polarized to depolarized power for circular illumination becomes

$$\frac{\text{Pol}}{\text{Depol}} = \frac{P_r + \frac{1}{2} P_S}{\frac{1}{2} P_S} = 2 \frac{P_r}{P_S} + 1 \quad . \tag{44}$$

Figure 19 is a plot of this ratio as a function of the ratio $P_S/(P_r + P_S)$. Comparison of the results in Fig. 7 with the curve in Fig. 19, shows that at 23-cm wavelength about 65 percent of the power returned at oblique angles of incidence is to be ascribed to the dipole scattering mechanism. A collection of randomly oriented dipoles illuminated with a linearly polarized wave will return 25 percent of the scattered power in the orthogonal mode. In this case, therefore, the ratio of polarized to depolarized power for circularly polarized waves becomes

$$\frac{\text{Pol}}{\text{Depol}} = \frac{P_r + \frac{3}{4} P_S}{\frac{1}{4} P_S} = 4 \frac{P_r}{P_S} + 3 \quad . \tag{45}$$

In Fig. 20 this polarization ratio is plotted as a function of the fraction of the total power scattered by dipoles. Comparison with Fig. 11 shows that again the fraction of the total scattered power that must be ascribed to the dipoles is in the vicinity of 70 percent. This agreement between the

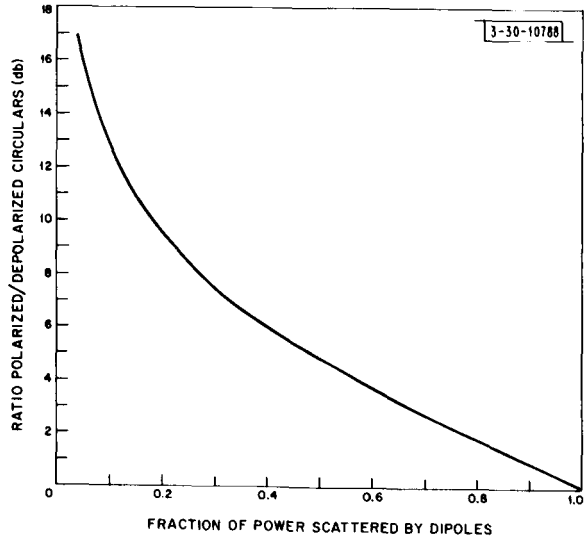

Fig. 19. Plot of ratio of polarized and depolarized power for circularly polarized illumination as a function of the fraction of power scattered by dipoles.

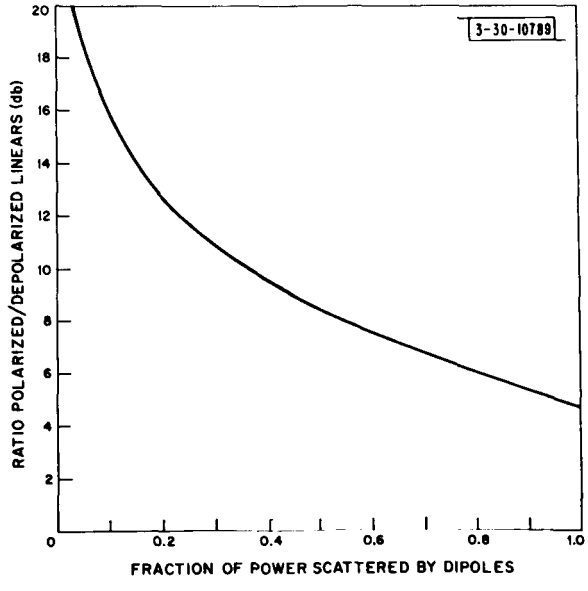

Fig. 20. Plot of ratio of polarized and depolarized power for linear illumination plotted as a function of the fraction of power scattered by dipoles.

conclusions drawn from linearly and circularly polarized data lends credence to the validity of the model assumed.

Our somewhat naive model of the scattering mechanism at oblique incidence is so far unable to account for a preferential backscattering when the E field is in the plane of incidence, as shown by the observational results of Figs. 15 and 16. At least two modifications may be made to the model to yield this effect. It may be that the dipoles behave as if oriented preferentially in the vertical direction on the lunar surface. An alternative model was suggested by Hagfors, et al. (1965), in the form of a tenuous layer covering the small-scale irregularities. The preferential scattering of waves with the E field in the plane of incidence was explained as a preferential transmission of these waves through the tenuous top layer. The latter model requires that a large fraction of the scatterers be buried underneath the tenuous layer. This assumption, unfortunately, does not appear to be in agreement with the recent Surveyor I and III pictures if these are to be considered as representative of the lunar surface in general. The most recent analysis of Surveyor I pictures indicates that the cumulative rock distribution is of the form*

$$N_1 = 5 \cdot 10^5 \cdot y^{-2.11} \tag{46a}$$

whereas the Surveyor III pictures appear to fit a law of the form*

$$N_3 = 3 \cdot 10^6 \cdot y^{-2.56} \tag{46b}$$

where N = cumulative number of grains per 100 m^2 and y = diameter of grains in mm. The number density of rocks or grains per m^2 with diameter between y and $y + dy$ is

$$n_1(y)\, dy = 1.055 \cdot 10^6 \cdot y^{-3.11}\, dy \tag{47a}$$

$$n_3(y)\, dy = 7.68 \cdot 10^6 \cdot y^{-3.56}\, dy \tag{47b}$$

while the geometric cross section of each grain expressed in m^2 is

$$\sigma_g = \frac{\pi}{4} y^2 \cdot 10^{-6} \quad . \tag{48}$$

Let us next assume that each grain has a radar cross section which is a certain constant fraction R of its geometrical cross section, when the diameter exceeds the wavelength, and zero otherwise. The cross section per unit area is, therefore, found to be

$$\sigma_1 = \frac{\pi R}{4}\, 9.59 \left\{ y_{min}^{-0.11} - y_{max}^{-0.11} \right\} \tag{49a}$$

$$\sigma_3 = \frac{\pi R}{4}\, 13.71 \left\{ y_{min}^{-0.56} - y_{max}^{-0.56} \right\} \quad . \tag{49b}$$

For y_{min} we may choose the wavelength of observation and for y_{max} we substitute a number large enough to make the last term in Eq. (49) vanish. The results are (note λ in mm!)

$$\sigma_1 = R \cdot 7.53 \cdot \lambda^{-0.11} \tag{50a}$$

$$\sigma_3 = R \cdot 10.77 \cdot \lambda^{-0.56} \quad . \tag{50b}$$

*"Surveyor III, A Preliminary Report," SP-146, National Aeronautics and Space Administration (June, 1967).

TABLE IV

COMPARISON OF OBSERVED AND COMPUTED CROSS SECTIONS PER UNIT SURFACE AREA

λ (cm)	Computed σ_1 (db)	Computed σ_2 (db)	Observed at $\phi = 40°$
68	−6.22	−17.42	−19.21
23	−5.70	−14.78	−17.43
3.8	−4.83	−10.39	−14.88

This is to be compared with the wavelength dependence observed in Sec. III.A.1, which is intermediate between the results of Eqs. (50a) and (50b). Assuming the reflectivity R to be the same as that of the moon as a whole, i.e., 0.065, we obtain the results shown in Table IV which also shows the cross section per unit surface area actually observed at an angle of incidence of 40°. It can be seen from this table that the number of rocks on the surface as derived from both the Surveyor I and Surveyor III pictures are more than enough to account for the return at oblique angles of incidence. Hence, if the areas photographed are typical of the lunar surface, the earlier interpretation of the radar data in terms of buried single scatterers [Hagfors, et al. (1965)] must be rejected, since the scatterers seen photographically rest largely on top of the surface rather than underneath. The presence of grains and rocks on top of the surface rather than buried inside the surface material, however, does not rule out the presence of a double layer surface model. It means only that the backscattering at oblique angles of incidence takes place without appreciable penetration of the top layer. The double layer model is still attractive in certain respects, both to explain a wavelength dependence of the quasi-specular return, as well as to account for the somewhat lower dielectric constant of the lunar surface material which is generally deduced from radiometric observations of the thermal emission from the moon (see Sec. IV).

IV. RADIOMETRIC OBSERVATIONS

The radiometric observation which has the most direct bearing on the question of the electrical properties of the lunar surface relates to the polarization of the thermal emission across the lunar disk. Plots of the degree of polarization observed as a function of offset from the center of the lunar disk are shown in Fig. 21, where the offset is measured in units of the lunar radius. In Fig. 22 the observations are compared with the curves to be expected on the basis of a transition from a homogeneous medium to vacuum. As can be seen, the fit is not very impressive. However, as shown in QPR (1966:4), the effect of the polar diagram is to depress the polarization curve for offsets in excess of 0.8. With this in mind one would deduce a dielectric constant of $\epsilon = 1.7$ from the data. Since this is completely incompatible with the reflectivity at normal incidence, some satisfactory explanation must be sought. In QPR (1966:4) it was suggested that surface undulations and a tenuous top layer could account for the discrepancy. The simple, homogeneous, tenuous top layer is effective in reducing the polarization at very oblique angles of incidence, say for offsets in excess of 0.8, but not for offsets less than 0.7 and it is difficult to

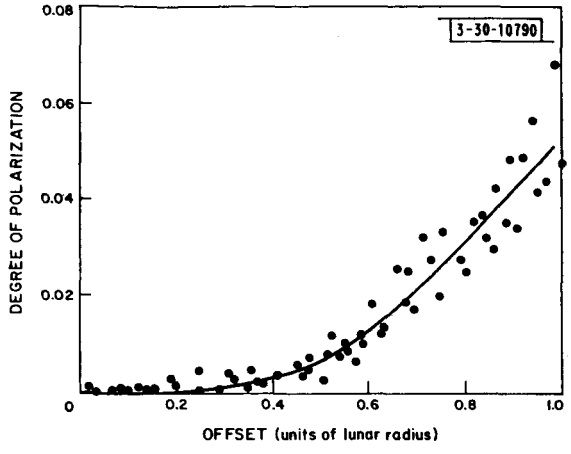

Fig. 21. Degree of linear polarization emitted by the moon as a function of antenna offset from the center.

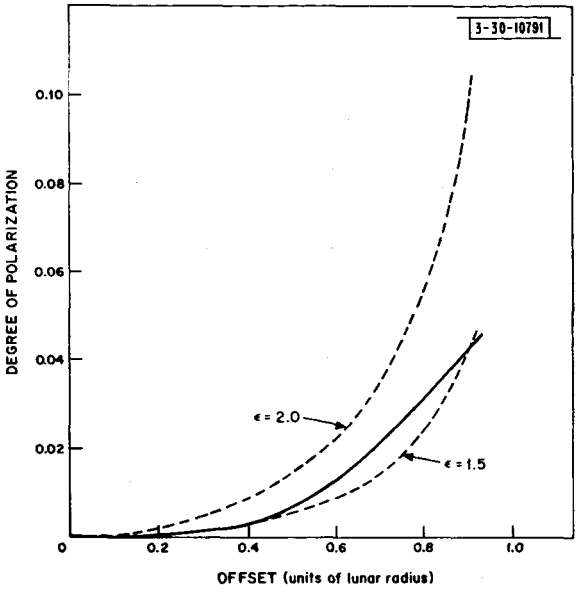

Fig. 22. Degree of linear polarization emitted by the moon as a function of antenna offset from the center compared with simple one-layer model.

reconcile the radar and the radiometric data on this basis alone. It may be possible to reach complete agreement on the basis of a more complicated surface structure such as the one discussed in connection with Eq. (11). The emission from such a layer has not yet been evaluated and presents an awkward mathematical problem. The presence of surface undulations may decrease the polarization of the emission somewhat as shown in QPR (1966:4), but far less than enough to account for the emission on the basis of a dielectric constant for the surface of 2.6 to 2.7. One further possibility which has not been discussed in previous reports results from the presence of rocks and pebbles on the surface which could emit unpolarized radiation. With a surface dielectric constant of 2.6 it would be required that 60 percent of the emission from the surface originate via an unpolarized mechanism in order for the polarization to be as low as is observed. This is considerably in excess of what one would expect on the basis of the radar data as well as from the Surveyor photographs. Quantitative agreement between radiometric and radar results, therefore, still seems to be lacking. It appears likely that a combination of the three mechanisms described must be invoked to reach quantitative agreement.

V. SUMMARY

The data obtained in this study together with earlier results have been shown to be compatible with a model of the lunar surface which is gently undulating and which is characterized by a mean slope of less than 10° when measured on the scale of tens of centimeters. The uppermost layers of this surface are compatible with a material having a relative dielectric constant not more than 2.6 with radiometric emission data tending to indicate a value lower than this. All the polarization data obtained by radar were explained on the basis of scattering from rocks or pebbles strewn over the basic, relatively smooth and undulating surface. It was shown that an amount of rock-like structure such as that observed in the Surveyor I and III photographs is quite adequate to

account for the scattering at oblique angles of incidence. Since the depolarized backscattered radiation is assumed to originate entirely from this structure, the strength of the backscattering at oblique angles of incidence appears to be a direct measure of the surface density of this material.

ACKNOWLEDGMENTS

The work of most of the technical personnel of Group 31, Surveillance Techniques, which operates the facilities of the Field Station, in preparing and conducting the work reported to date is gratefully acknowledged, as is the work of members of Group 46, Microwave Components, in cooperating with Dr. McCue on the 8.6-mm radar.

The use of the facilities of the Lincoln Laboratory Millstone-Haystack complex, provided by the U.S. Air Force, is also gratefully acknowledged.

REFERENCES

Beckmann, P., "Scattering by Composite Rough Surfaces," Report 4, Dept. of Elec. Eng., Univ. of Colorado (1964).

Beckmann, P., private communication (1967).

Evans, J. V., "Radar Studies of the Moon," J. Res. Natl. Bur. Standards, Radio Science 69D, 1637-1659 (1965).

Evans, J. V., and Pettengill, G. H., "The Scattering Behavior of the Moon at Wavelengths of 3.6, 68 and 784 Centimeters," J. Geophys. Res. 68, 423-447 (1963).

Evans, J. V., and Hagfors, T., "Study of Radio Echoes from the Moon at 23 Centimeters Wavelength," J. Geophys. Res. 71, 4871-4889 (1966).

Grieg, D. D., Metzger, S., and Waer, R., "Considerations of Moon-Relay Communication," Proc. IRE 36, 652-663 (1948).

Hagfors, T., "A Study of the Depolarization of Lunar Radar Echoes," Radio Science (New Series) 2, 445-465 (1967).

Hagfors, T., Brockelman, R. A., Danforth, H. H., Hanson, L. B., and Hyde, G. M., "Tenuous Surface Layer on the Moon: Evidence Derived from Radar Observations," Science 150, 1153-1156 (1965).

Hughes, V. A., "Diffraction Theory Applied to Radio Wave Scattering from the Lunar Surface," Proc. Phys. Soc. (London) 80, 1117-1127 (1962).

Kerr, F. J., and Shain, C. A., "Moon Echoes and Transmission Through the Ionosphere," Proc. IRE 39, 230-242 (1951).

Pettengill, G. H., and Thompson, T. W., private communication, (1967).

Rea, D. G., Hetherington, N., and Mifflin, R., "The Analysis of Radar Echoes from the Moon," J. Geophys. Res. 69, 5217-5223 (1964).